Available online at www.sciencedirect.com
ScienceDirect
Cement and Concrete Research 36 (2006) 1453 – 1459
Cement and Concrete Research

Use of computer assisted image analysis for the determination of the grain-size distribution of sands used in mortars

G. Mertens *, J. Elsen

Afdeling Geologie, Katholieke Universiteit Leuven, Celestijnenlaan 200E, 3001 Heverlee, Belgium

Received 22 August 2005; accepted 8 March 2006

Abstract

A quantification procedure for constructing the sieving curves of sands used in mortars, from two-dimensional data obtained by image analysis of thin sections, has been developed. To test the suitability of this procedure, thin sections were made from ten fluorescent epoxy-impregnated mortars, containing five different sands of which the sieving curves had previously been determined. Whereas previous investigations were typically based on independent and individual micrographs, a new approach has been adopted in which measurements are performed on single composite images. Two stereological models, based on cubic and spherical particles respectively are applied to the examples and the results compared with the sieving curves. The results obtained show a reliable congruence, especially for the spherical model and when shape factors of sectioned grains are high. Sieving curves and grain-size distribution curves established from image analysis may have virtually the same precision, but the latter has a lower reproducibility.

Keywords: Image analysis; Particle size distribution; Aggregate; Mortar

1. Introduction

Historical mortars have two main components: the binder, which is usually lime or hydraulic lime, and the aggregate [1], which in most cases consists of a locally available sand [2]. Knowledge of the grain-size distribution of the aggregate in these mortars, which plays an important role for restoration applications, is invaluable [3]. Combined with the volume fraction of aggregate used, this is necessary for designing compatible mortars. Furthermore, the sieving curve of a sand is a fingerprint of the geological formation from which the sand is taken, so that it is an important tool for tracing the origin of the raw materials [4]. A generally applied method of establishing the grain-size distribution of the sand is to attack chemically the mortar sample with an appropriate acid [5]. The binder is dissolved and the insoluble residue is used to construct the sieving curve. However, part of the aggregate may not be resistant to the acid attack and readily dissolve [6,7]. The large amount of sample required [8] is an additional restriction of this method. A different approach is required to obtain reasonable results when only a limited amount of sample is present. Image analysis of thin sections can overcome the limitations of the acid-attack method. Traditional optical or scanning electron microscope (SEM) images can be processed by image analysis methods to allow measurement of the sectioned grains. Well-established stereological calculations are used to convert these 2D data to the required 3D values [9,10].

In most studies, data are acquired from analysis of a set of individual images [6,11]. For statistical reasons, these single images need to be taken in an arbitrary and independent manner. An intrinsic problem of this approach is that, due to the limited resolution of digital cameras, small grains cannot be detected and measured. A possible solution is to choose a higher magnification, but this increases the edge effects, so those larger objects may not entirely lie within the field of measurement. Hence, larger grain-size populations are underestimated. The great spread of particle sizes is the most important difficulty to overcome. The proposed approach deals with this problem by making measurements on single composite pictures made up of a large set of individual images. In this way, edge effects are reduced without any loss of resolution and many particles are

* Corresponding author. Tel.: +32 16 327586; fax: +32 16 327981.
E-mail address: Gilles.Mertens@geo.kuleuven.be (G. Mertens).

0008-8846/$ - see front matter © 2006 Elsevier Ltd. All rights reserved.
doi:10.1016/j.cemconres.2006.03.004

Table 1
The table shows the type of sand, the surface area of the digitised frame, the number of micrographs assembled, the number of objects in the measuring frame and the mean shape factor (cf. infra) of the objects in each thin section

Sample	Sand	Surface area (cm^2)	# Micrographs	# Objects	Mean shape factor (Q)
M01	Rhine sand	5.08	285	4237	0.7060
M02	Rhine sand	4.69	300	4008	0.6822
M03	Fine scouring sand	1.05	150	6122	0.6699
M04	Fine scouring sand	1.33	145	6387	0.6844
M05	Random sand 0/4	3.67	198	5548	0.7319
M06	Random sand 0/4	3.84	247	5126	0.7078
M07	Random sand 0/2	5.09	342	10206	0.7186
M08	Random sand 0/2	2.33	150	3641	0.7122
M09	Normalised sand	3.91	208	6203	0.7049
M10	Normalised sand	4.36	289	6648	0.7010

simultaneously measured, giving statistically reliable results. These show that the quantification procedure is successful. However, besides the effectiveness of the new approach, some limitations on the stereological probability distribution for homogeneous sands remain. Variability in grey-level distributions and a need for visual inspection of the composite images limit the method to be used in a non-automated procedure.

2. Experimental procedure

Ten mortar samples were prepared using five different sands (Table 1) according to Belgian standard NBN 771-10, which is currently used for the preparation of cement-based mortars. Since the procedure is oriented towards the application to ancient (mainly lime) mortars, hydraulic lime (Unilit TD 13N) was preferred to Portland cement as a binder. After drying, the samples were twice impregnated under vacuum with a fluorescent (FITC) dyed epoxy resin to enhance the contrast between the sand grains and the inter-granular space. Thin sections with a thickness of 30 μm were prepared from these mortar samples.

The micrographs were acquired with an Evolution LC digital camera attached to a Zeiss petrographical microscope. The images, which have a resolution of 833 pixels/mm, were made using a Zeiss 5X objective and incident fluorescent light. Subsequently, the micrographs were processed with the Image Pro Plus® software package. To verify the pertinence of the image analysis approach, comparison with another valid technique is necessary. Sieving analysis is probably the most widespread, generally accepted and easiest way of collecting information on the grain-size distribution of aggregates. For the five sands used as aggregates, the sieving curves (Fig. 1) have been established according to Belgian Standard NBN B 11-013.

3. Procedure

3.1. Image treatment

For the micrographs acquired in the RGB colour model (Fig. 2A), the intensity channel (Fig. 2B) has been calculated according to the following formula:

$$I = \frac{R + G + B}{3} \quad (1)$$

This gave the best contrast between aggregates and the inter-granular space, facilitating the thresholding operation (Fig. 2C). Additional image treatment before binarisation was unnecessary since the arbitrary boundary between grey-level of aggregates and matrix can be easily distinguished. This is shown in the pixel intensity profile in Fig. 2(B2). However, thin sections are strictly speaking not 2D sections. The section of a particle in the lower

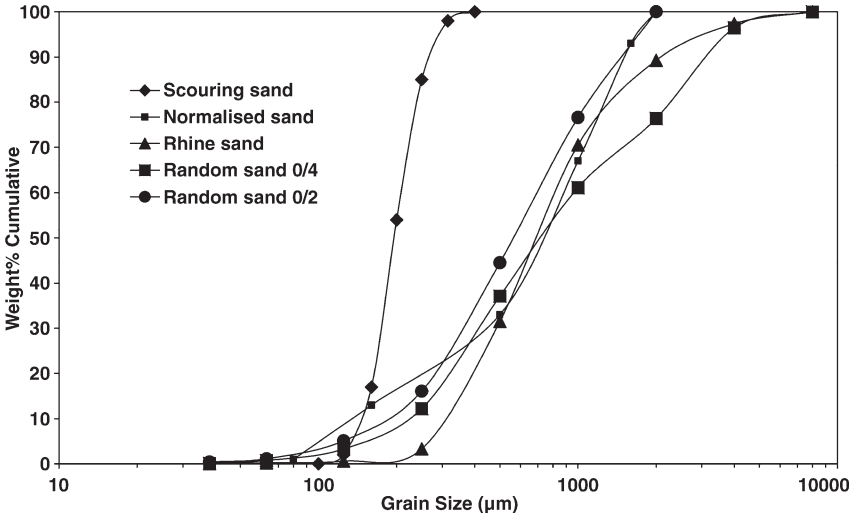

Fig. 1. Grain-size distributions of the aggregates determined by sieving.

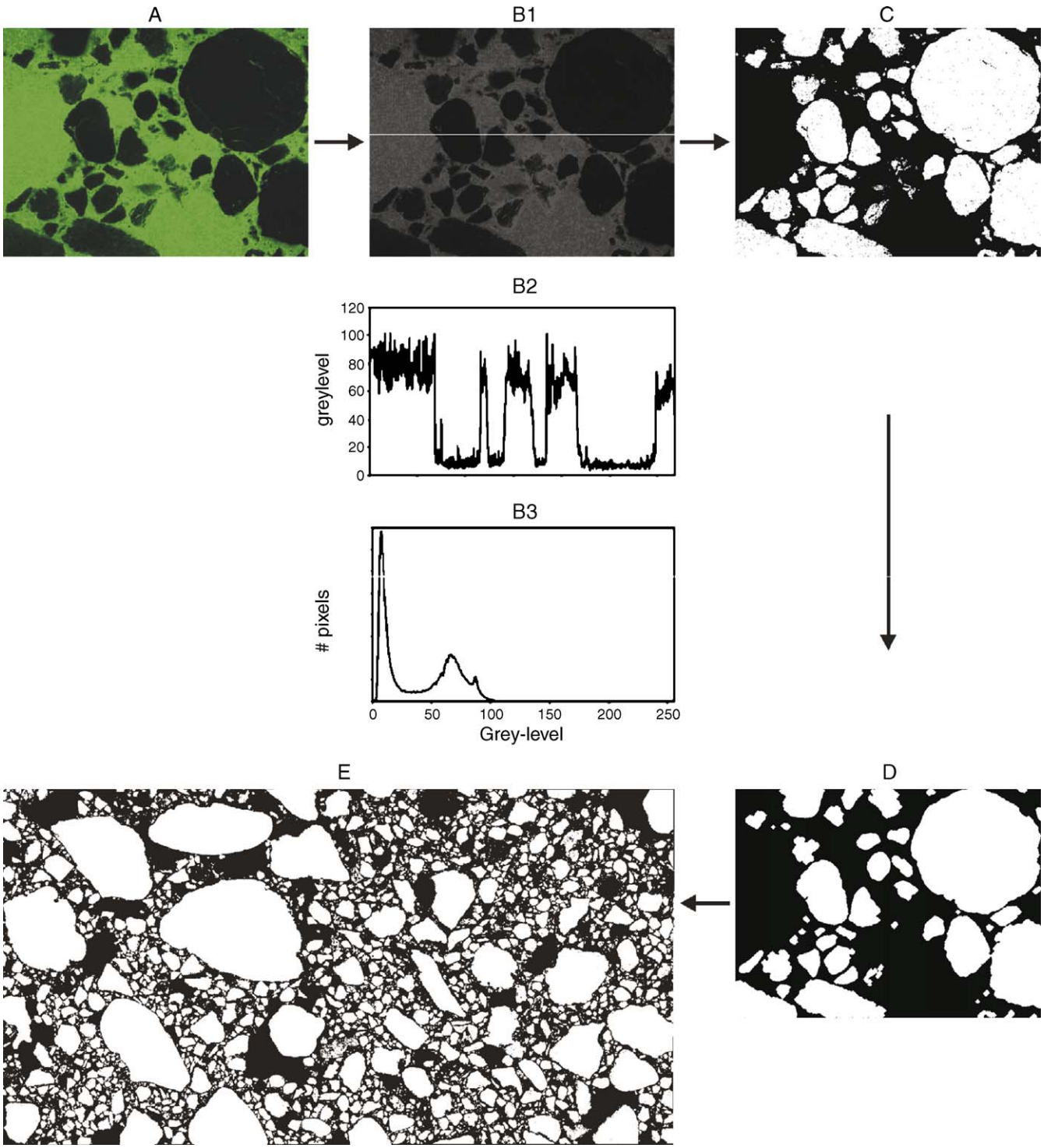

Fig. 2. Flowchart of the image treatment: (A) Colour image (incident fluorescent light). (B1) Intensity channel from A with (B2) profile through the micrograph and (B3) the grey-level histogram. (C) Black and white image after thresholding. (D) Black and white image after the despeckle, erosion and dilation operation and after filling of the holes. (E) Composition of a single picture. Frame width: 1.5 mm for images A–D, 26 mm for image E.

plane of the 30 μm thick slice might differ significantly from its section in the upper plane. Some particles may cross the lower and not the upper part of the thin section, so that they are in a twilight zone between the light intensity levels of the aggregate and the inter-granular space. No correction was made to reduce the influence of this effect. For micrographs where the distinction of phase boundaries is less evident, frequency filters [12] or separation techniques based on texture filtering [13] can be used. The threshold value was kept the same for all micrographs from the same thin section. However, due to small differences in thickness or preparation conditions, a different value was needed for each thin section. After the binarisation

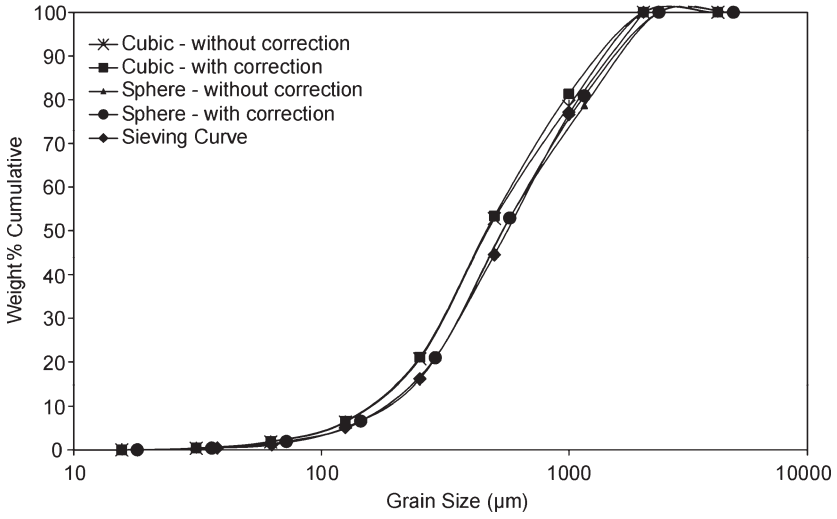

Fig. 3. Sieving and calculated curves of M08.

operation, a despeckling filter was applied to all micrographs. This convolution filter reduces noise. This reduction can also be done by composing an image as an average of multiple frames from the same area [14]. However, this is a time consuming operation and does not ensure that small artefacts such as cracks are removed from the image. In addition, the succeeding erosion and dilation operations help to reduce noise and the effect of small artefacts. Application of these two morphological filters has the benefit of separating touching grains. Moreover, the irregularly shaped grain boundaries are flattened, giving a more reliable perimeter for the shape factor calculation. The shape factor (Q) is calculated according to the following formula:

$$Q = \frac{4\pi A}{U^2} \tag{2}$$

In this formula, A represents the area and U the perimeter of the sectioned grain. The shape factor varies from 1 for circular objects to nearly 0 for irregularly shaped objects. As in most studies [15], it is only used to give a qualitative idea about the morphology of the populations. Erosion operations can influence grain-size distributions, principally affecting the finer fraction [6]. However, the results show that there is no tendency to underestimate the calculated weight proportion of the finer fraction.

In the next step, all micrographs, with slightly overlapping borders, are fitted to create a single composite image (Fig. 2E). At this stage, some particles still have to be separated manually and the holes of porous particles need to be filled up. Finally the objects are counted and measured. No automated procedure, by means of a macro-program, has been developed, since some interaction with the software is required during processing. The automated fit, used to create a single micrograph, requires visual inspection since poor matches may occur and a consequent adjustment of the parameters may be necessary. Furthermore, separation of contiguous grains in the final step needs to be done manually, since automated techniques such as watershed did not work satisfactorily. Recently, promising new techniques have been developed [16] to separate touching objects. However, they are not yet implemented in this work. Moreover, the threshold-value for each thin section needs to be chosen after visual evaluation.

3.2. Stereology

It is necessary to choose the right 2D parameter for the calculation of the 3D grain-size distributions. In the proposed model, calculations are based on the maximum Feret diameter. This choice results from the application of the stereological calculations taken from Sandström [9] whose model is based on results taken from Exner [10]. The maximum Feret diameter is the maximum distance between two parallels tangent to the 2D-object [17]. Since there is no evident relationship between a random 2D section of an arbitrary particle and its behaviour in a sieving analysis, some assumptions are necessary. First, it is important to choose a representative particle shape [18]. Two particle shapes are proposed; one spherical and the other cubic. Particle size and shape are considered to be independent. Furthermore, the model assumes uniform and random sections, selected throughout as uniform and random mortar samples. For an arbitrary 2D section

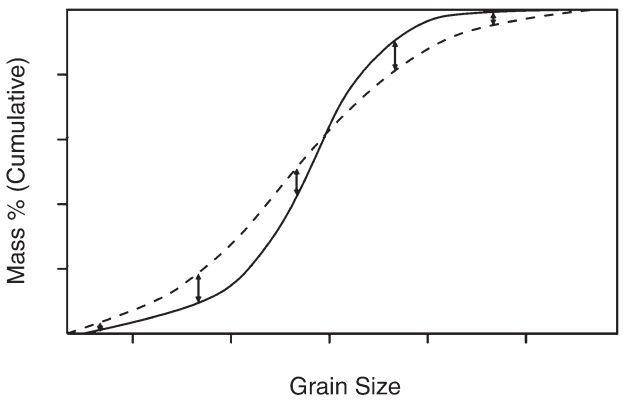

Fig. 4. Calculation of the differences between two grain-size distribution curves.

through a sphere of diameter R, the probability that the 2D diameter lies between r and $r+\mathrm{d}r$ is:

$$p_i = \sqrt{1-\left(\frac{r+\mathrm{d}r}{R}\right)^2} - \sqrt{1-\left(\frac{r}{R}\right)^2} \quad (3)$$

Since the aggregate is not composed of a series of spheres of identical diameter, the number of objects in each 3D grain-size class (N_{v_1}, N_{v_2}, ...) is given by the following system of equations [19]:

$$\begin{bmatrix} p_1 & 0 & 0 & 0 \\ p_2 & \ddots & 0 & 0 \\ \vdots & \ddots & \ddots & 0 \\ p_n & \cdots & p_2 & p_1 \end{bmatrix} \cdot \begin{bmatrix} N_{v_1}.D_1 \\ N_{v_2}.D_2 \\ \vdots \\ N_{v_n}.D_{n_1} \end{bmatrix} = \begin{bmatrix} N_{a_1} \\ N_{a_2} \\ \vdots \\ N_{a_n} \end{bmatrix} \quad (4)$$

Knowing the number of 2D sectioned grains in each class (N_{a_1}, N_{a_2}, ...) it is possible to calculate the probable number of grains in each 3D grain-size class. For cubic objects, the diameter D can be replaced by the mean calliper diameter H [20]. This is the average distance between two parallel planes when a specific 3D object is placed in between in an arbitrary manner. For a cube, this value, normalised with regard to the maximum length, is $\frac{1.5}{\sqrt{3}}D$ (with D its edge length). The probability distribution of the maximum Feret diameter for cubic particles can be found in Sandström [9].

3.3. Edge effects

Efforts have been made to find adequate corrections for edge objects [9,19]. These are objects crossing the borders of the measuring frame. If no corrections are applied, the size of these objects is systematically underestimated. Large objects have a higher probability of intersecting margins, thereby necessitating important corrections and causing the results to be less reliable. Some authors [6] prefer to make no corrections. In this study, edge effects are reduced as much as possible by choosing a large measuring frame compared to the size of the largest particles present, but still using a reasonable resolution. There are different methods of correcting for edge objects. In this study, one of the models from Russ [19] has been chosen. It is based on the size of the measuring frame and the objects in each specific grain-size class according to the following formula:

$$\text{Correction factor} = \frac{W_x \cdot W_y}{(W_x - F_x)\cdot(W_y - F_y)} \quad (5)$$

W_x Frame width
W_y Frame height
F_x Object width
F_y Object height

The correction factor becomes very important when objects are larger than half the measuring frame size [9]. Since this is not the case in any of the examples, the method can be reliably used. Beside the calculations considering all objects and using no corrections, the same set of data, without edge objects, is treated using the correction method above. Both results are compared and the influence of the corrections is verified experimentally.

Table 2
Mean absolute differences between the curves in terms of percentages

	Sphere — with correction	Cube — with correction	Sphere — without correction	Cube — without correction
Differences between the calculated and the sieving curves				
M01	3.43	3.50	3.13	3.56
M02	1.35	3.10	1.15	4.35
M03	6.10	9.95	6.15	10.29
M04	4.85	9.43	6.45	7.90
M05	1.90	1.65	0.49	2.58
M06	7.51	5.27	3.70	2.79
M07	2.59	5.78	4.31	4.46
M08	0.81	3.45	1.08	2.77
M09	1.57	3.00	1.53	2.86
M10	1.43	3.84	1.66	3.87
Mean calculated difference				
M01 and M02	2.39	3.30	2.14	3.96
M03 and M04	5.48	9.69	6.30	9.10
M05 and M06	4.71	3.46	2.09	2.69
M07 and M08	1.70	4.61	2.70	3.61
M09 and M10	1.50	3.42	1.59	3.37
Mean difference curves				
M01 and M02	2.37	2.95	1.75	2.84
M03 and M04	5.48	9.69	6.30	9.10
M05 and M06	4.71	3.05	2.09	1.43
M07 and M08	1.59	4.61	2.63	3.42
M09 and M10	0.89	3.17	1.04	3.09
With respect to each other				
M01–02	2.72	2.98	4.08	4.48
M03–04	1.25	1.26	2.39	2.39
M05–06	5.61	6.19	3.38	4.12
M07–08	2.18	2.34	3.62	2.08
M09–10	1.38	1.34	1.55	1.55

4. Results and discussion

From each thin section of the ten mortar samples (five different sands), four different curves were calculated; for the spherical and the cubic model, with and without correction for edge objects. As an example, the calculated grain-size distributions based on image analysis are shown together with the sieving curve of sample M08 in Fig. 3.

To attribute a mathematical value to the divergence, the mean difference between the calculated and theoretical curves was

determined. Different statistical methods were tested, but none of them gave satisfactory results. We preferred a method whereby a calculated value reflects the visual correspondence of the two curves. More specifically, it expresses their mean difference in terms of percentages (Fig. 4). In practice, at least five pairs of points with the same abscissa are chosen on both curves and their absolute difference is calculated. The points are equally spaced on a logarithmic scale. The sum of these results is normalised with respect to the number of points.

The mean differences between the calculated curves and the sieving curves are presented in Table 2. In addition, the difference with respect to the sieving curves of the 'mean difference curves' is also presented. These are the curves based on the arithmetic average of the absolute cumulative class sizes of mortars made from the same sand. If we compare these values with the 'mean calculated difference' (average of the mean difference of both curves made from the same sand), it is possible to verify the influence of a larger measuring frame on the 'goodness-of-fit'. Table 2 also includes the values of the differences of the calculated curves from two mortars with the same sand, with respect to each other. In this way, the reproducibility of the measurements can be verified.

Table 2 shows that the correspondence is rather good for most samples. Generally, the spherical model without corrections gives the best results, even if the mean shape factor (Table 1) is closer to that of cubic particles. 2D circular sections have shape factors of 1, whereas 2D sections through cubic particles have a mean shape factor of 0.668. However, in Fig. 5, we can see that the fit between the calculated and the sieved curves is better if the mean shape factor is high. This can be explained by the fact that thin sections with objects of low symmetry have a low mean shape factor. As a consequence, the differences with respect to the sieving curves are larger since the calculated curves are based on models of highly symmetrical forms.

For homogeneous, subspherical and 'clean' quartz-arenitic sands, the curves based on image analysis will probably better match the sieving curves than those for 'dirty' sub-angular sands with a diverse mineralogy [11]. This is the case for M05–M06–M07–M08 where porous particles are present. In the weight calculations of the grain-size classes, they are considered to be massive and to have an identical density to the other particles. In the sieving analysis on the contrary, they will lower the proportion of the corresponding grain-size class, because of their lower density. Technical imperfections can also cause divergences. As discussed previously, no correction was made for the effects related to thin section thickness. Particles with a different section in the upper and lower plane of a thin section may be classified in the wrong grain-size class and affect the results. From Table 2, it is clear that in general, the grain-size distribution curves corrected for edge objects fit the sieving curves less than to those without corrections. When corrections are unfavourable for the 'goodness-of-fit', this is usually due to an overestimation of the number of larger grains. This aberration could be due to a non-uniform distribution of larger grains over the measuring frame. Most thin sections cross the border of the mortar samples, whereby most grains lie entirely within the measuring frame. Hence, the corrected weight fractions are overestimated, especially for larger objects. Table 2 shows that 13 out of 20 'mean difference curves' give better results than the corresponding 'mean calculated difference' meaning that the use of several thin sections improves the counting statistics.

If we compare the grain-size distribution curves of mortars made with the same sand, we see that the reproducibility is satisfactory, even if it is better in only 11 out of 20 examples, compared to the 'mean calculated differences'. Therefore, we suggest that there is hardly any difference between a curve established by sieving and a curve obtained by image analysis, despite the limitations of the latter technique. However, the image analysis results show a greater spread, even if both methods may virtually have the same precision, with M03 and M04 exceptions to this. Their calculated curves do not fit well the sieving curves, but they are easily reproducible. The origin of the deviation is systematic. The sand used in these mortars is very homogeneous whereas the model is based on probabilities

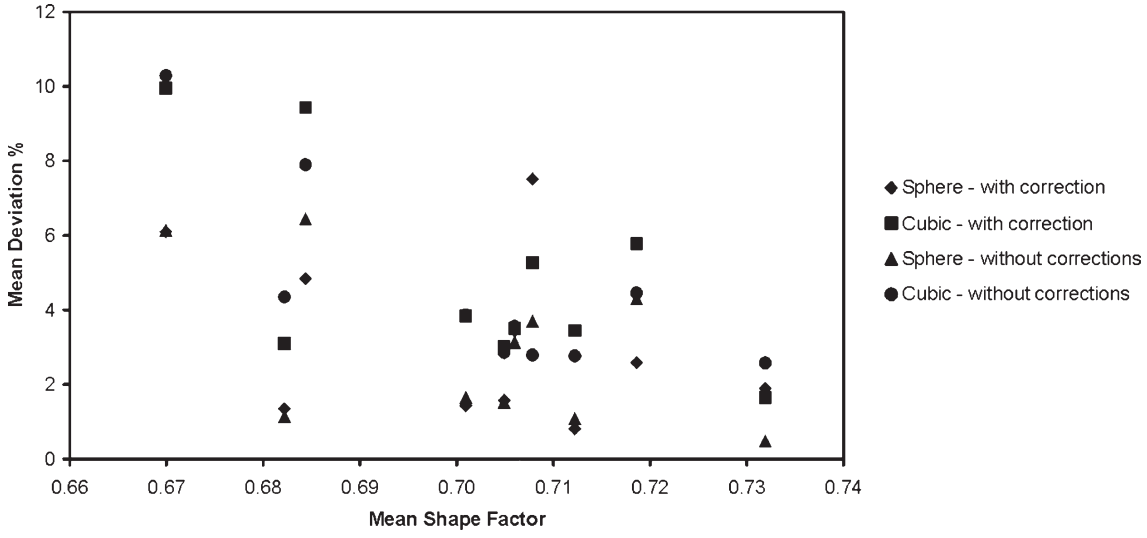

Fig. 5. Mean difference between the calculated curves and the sieving curves versus mean shape factor.

established for a continuous grain-size distribution [21]. In the model, the largest sections will be partly treated as a smaller section of larger grains, biasing the results.

5. Conclusions

Image analysis of micrographs taken from thin sections has been tested as a tool to recover the grain-size distribution curves of sands used in mortars. The results from the analyses of ten self-made mortars are consistent with the results from the sieving analysis of the sands. The image analysis method involves two main steps. The particularity of the first step, the image treatment, is to measure 2D-parameters on composite images. This approach reduces the errors induced by edge effects. In the second step, stereological calculations are performed on the measured 2D-parameter distribution. Two stereological models, based on spherical and cubic particles respectively, have been tested. The image analysis results obtained with the first method show a better correlation with the sieving curves, especially when form factors of sectioned grains are high. Even though some changes to the stereological model are necessary when dealing with homogeneous sands, the method is very promising as a tool for the determination of the grain-size distribution of sands used in mortars.

Acknowledgements

The first author is currently working as an Aspirant of the Flemish Fund for Scientific Research (FWO), which is kindly acknowledged for its financial support. The authors are very grateful to Jan-Eric Lindqvist for providing detailed information on his stereological model calculations.

References

[1] A.B. Leslie, J.J. Hughes, Binder microstructure in lime mortars: implications for the interpretation of the analysis results, Quarterly Journal of Engineering Geology and Hydrogeology 35 (2002) 257–263.
[2] P. Swallow, D. Carrington, Limes and lime mortars — part I, Journal of Architectural Conservation 1 (3) (1975) 7–25.
[3] A. Moropoulou, A. Bakolas, K. Bisbikou, Investigation of the technology of historic mortars, Journal of Cultural Heritage 1 (2000) 45–58.
[4] M. Franzini, L. Leoni, M. Lezzerini, A procedure for determining the chemical composition of binder and aggregate in ancient mortars: its application to mortars for some medieval buildings in Pisa, Journal of Cultural Heritage 1 (2000) 365–373.
[5] A. Coutelas, L. Guyard, Ch. David, Pétroarchéologie de mortiers gallo-romains: application de méthodes analytiques à l'étude des thermes du Vieil-Evreux (Eure), Les nouvelles de l'archéologie 81 (2000) 31–36.
[6] J.E. Lindqvist, M. Sandström, Measurement of aggregate size distribution using image analysis in light microscopy, SP REPORT 31 (1997) 1997.
[7] J.I. Alvarez, A. Martìn, P.J. García Casado, I. Navarro, A. Zornoza, Methodology and validation of a hot hydrochloric acid attack for the characterization of ancient mortars, Cement and Concrete Research 29 (1999) 1061–1065.
[8] B. Middendorf, G. Baronio, K. Callebaut, J.J. Hughes, Chemical–mineralogical investigations of old mortars, in: P.J.M. Bartos, C.J.W.P. Groot, J.J. Hughes (Eds.), Proceedings of the RILEM International Workshop "Historic mortars: Characteristics and tests", 1999, pp. 53–61, (Paisley).
[9] M. Sandström, Determination of the size distribution of aggregates by computer assisted image analysis, SP REPORT 52 (1995) 1995 (Borås, Sweden).
[10] H.E. Exner, Analysis of grain and particle-size distributions in metallic materials, International Metallurgical Reviews 17 (1972) 111–127.
[11] D. Lagrou, R. Dreesen, L. Broothaers, Comparative quantitative petrographical analysis of Cenozoic aquifer sands in Flanders (N Belgium): overall trends and quality assessment, Materials Characterization 53 (2004) 317–326.
[12] M. Barrioulet, R. Saada, E. Ringot, A quantitative structural study of fresh cement paste by image analysis Part 1: image processing, Cement and Concrete Research 21 (1991) 835–843.
[13] M.A. Werner, D.A. Lange, Quantitative image analysis of masonry mortar microstructure, Journal of Computing in Civil Engineering 13 (2) (1999) 110–115.
[14] E. Anselmino, A. Miroux, S. van der Zwaag, Dispersoid quantification and size distribution of hot and cold processed AA3103, Materials Characterization 52 (2004) 289–300.
[15] J. Ravier, Tentative de quantification de la forme des particules, Bulletin de Liaison des Laboratoires des Ponts et Chaussées 157 (1988) 39–46.
[16] E.H. van den Berg, A.G.C.A. Meesters, J.A.M. Kenter, W. Schlager, Automated separation of touching grains in digital images of thin sections, Computers and Geosciences 28 (2002) 179–190.
[17] P. Besançon, B. Fosse-Lemarchand, A. Lafaye, Granulométrie par croisement de la microscopie et du tamisage, Bulletin de Liaison des Laboratoires des Ponts et Chaussées 157 (1988) 47–55.
[18] R. McAfee, I. Nettleship, The simulation and selection of shapes for the unfolding of grain size distribution, Acta Materialia 5 (2003) 4603–4610.
[19] J.C. Russ, Computer-Assisted Microscopy: The Measurement and Analysis of Images, Third edition, Plenium Press, New York, 1990.
[20] E.E. Underwood, Quantitative Stereology, Addison-Wesley, Reading, Massachusetts, 1970.
[21] J.E. Lindqvist, M. Sandström, Determination of the size distribution, sieve curve, for aggregates using optical microscopy, in: H. Pietersen, J. Larbi, H. Janssen (Eds.), Proceedings of the 7th International Euroseminar on Microscopy Applied to Building Materials, Delft, 1999, pp. 297–305.